JOURNAL OF MATERIALS SCIENCE 31 (1996) 5837–5847

# Complex image generation in the laser scanning confocal microscope of a polymer blend system

A. E. RIBBE, T. HASHIMOTO*†
*Department of Polymer Chemistry, Graduate School of Engineering, Kyoto University, Kyoto 606-01, Japan*
H. JINNAI
*†Hashimoto Polymer Phasing Project, ERATO, JRDC, Morimoto-cho, Simogamo, Sakyo-ku, Kyoto 606, Japan*

The structure formation of a binary polymer blend of poly(styrene-*ran*-butadiene) and polybutadiene is investigated by laser scanning confocal microscopy (LSCM). The contrast generation of spherical and interconnected morphologies is discussed in detail and compared to that obtained by transmission electron microscopy. From the LSCM three-dimensional modelling of a bicontinous structure is performed.

## 1. Introduction

To obtain real space information about the morphology of polymer blend systems, especially the structure development during the phase separation known as spinodal decomposition (SD), a number of microscopic methods, for example, transmission electron microscopy (TEM), scanning electron microscopy (SEM), and light microscopy (LM) have been utilized.

TEM allows observation of structures down to nanoscale but requires complicated and time consuming sample preparation and the information on the picture is reduced to a two-dimensional reproduction of a space filling morphology (see for example Kim *et al.* [1]). With scanning electron microscopy only the surface of a sample can be investigated. By using the etching technique, as presented by Shabana *et al.* [2] the inner structure of a specimen can be made visible.

By selective staining of the polyisoprene with iodine the morphology of the polyisoprene/polybutadiene blend system could be made visible by LM as presented by Laeuger *et al.* [3]. Computer simulations concerning the structure evolution during SD have also been presented by Oono *et al.* [4], Yeung [5], Furukawa [6], Kotnis and Muthukumar [7], Koga and Kawasaki [8], and Takenaka and Hashimoto [9].

The laser scanning confocal microscopy (LSCM), a special application of the light microscope, has been up to now mainly used in materials and biological research [10]. This technique usually needs no special treatment of the sample. The lateral resolution of a light microscope is limited by the wavelength of the light source but is improved in the LSCM by using the scanning technique to about one half the size of the wavelength. A laser beam, which is focused by an objective lens on the sample, is scanned in the horizontal direction and the reflected light is passed back through the objective lens to be registered by a detector system, which is usually a photomultiplier. By introducing a pinhole in the back focal plane, a certain fraction of the back-scattered light, up to a definite scattering angle $\alpha$, can pass through the aperture. Images of slices with small focal depth leading to high contrast and resolution are obtained [11]. Therefore, this technique makes it possible to scan subsequent slices with a focal depth depending on the magnification and pinhole size. By moving the sample in a direction vertical to the scanning direction a series of images are obtained from which the three-dimensional morphology can be reconstructed. Examples of the application using a polymer system was presented recently by Verhoogt *et al.* [12], Li *et al.* [13] and Jinnai et al. [14].

In this paper the image generation in the LSCM of a polymer blend of poly(styrene-*ran*-butadiene) (SBR) and polybutadiene (PB) is presented and compared with that of conventional transmission electron microscopy. A number of reciprocal space analyses have been done by Hashimoto *et al.* [15–19] using this system, especially in relation to spinodal decomposition [20], a phase separation process and mechanism for thermodynamically unstable mixtures. This paper will be restricted to the discussion of the image interpretation of this structure with LSCM and TEM. A discussion of the phenomenon with the comparison of the real and reciprocal space analysis will be the topic of a forthcoming paper [21].

## 2. Experimental procedure

The polymers SBR and PB have weight average molecular weight of $M_W$ of $1.79 \times 10^5$ and $2.23 \times 10^5$,

* Author to whom correspondence should be addressed.

0022–2461 

respectively, and heterogeneity indices, $M_W/M_n$ of 1.2 and 1.3, respectively. The SBR contains 20 wt % of styrene comonomer units determined by nuclear-magnetic resonance (NMR). The microstructure of butadiene part as determined by NMR: for the SBR, 1,4-cis 17%, 1,4-trans 31%, 1,2-vinyl 52% and for the PB, 1,4-cis 23%, 1,4-trans 37%, 1,2-vinyl 40%.

The two polymers were dissolved in toluene to make a 5 wt % polymer in solution. Binary mixtures with compositions of SRR/PB 40/60, 50/50 and 70/30 wt/wt were cast in petri dishes. The solvent was allowed to evaporate over 1 week at 30 °C. The 0.15 mm thick samples were further dried in a vacuum oven until no further mass loss could be observed.

For homogenization, a mechanical mixing process, "Baker's transformation", is applied, as the $T_c$ of the system with an upper critical solution temperature (UCST) phase diagram is very high (> 140 °C). This mixing procedure leads to a homogeneous polymer blend which shows spinodal decomposition. Details are described elsewhere [22, 23].

For LSCM and light scattering examination no special treatment of the sample was required. LSCM measurements were performed with a LSM 320 (Zeiss) using a He/Ne laser with $\lambda = 633$ nm wavelength and image processing was done using software supplied by Zeiss. All images were recorded in reflection mode. The focal depth of the images are given in the respective figure legends. A photomultiplier is used as a detector. A detailed description can be found in the literature [11].

For the projection onto z,x- and z,y-plane a number of slices (typically 30) were mounted one upon the other as shown in Fig. 1, where the coordinate $O_{x,y,z}$ is fixed to the laboratory. For a three-dimensional reconstruction the single slices were first noise-reduced by applying a two-dimensional smoothing function.

A "sandwich" of pure SBR and PB was prepared and annealed at 100 °C for 5 min under slight pressure. Thus a sample with a single SBR/PB interface could be obtained (see Fig. 2).

For TEM investigations the samples were cut using low temperature ultramicrotomy at − 100 °C and the ultra-thin sections were stained with $OsO_4$ vapour at room temperature. A TEM (Hitachi H-600) with 100 kV acceleration voltage was used.

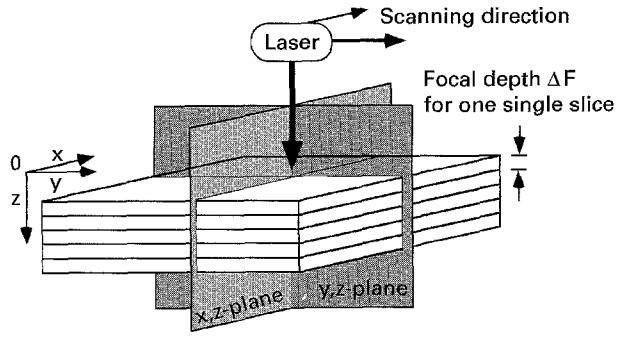


*Figure 1* Schematic illustration of the scanning geometry of a LSCM. The direction of the incident beam corresponds to the z-direction and film specimens were placed onto the microscope stage (x,y-plane). The single slices may not necessarily have an exactly common limit (overlap region) as discussed in the text.

## 3. Results and discussion

### 3.1. Single SBR/PB interface

Figs 2c and d show the LSCM images of a single interface of pure SBR and pure PB welded together. The white line corresponds to back-scattered light from the macroscopic interface caused by the refractive index difference between SBR and PB, whereas the two pure homopolymers appear dark in the original obtained by a LSCM scan (Fig. 2c). By maximum enhancement of the contrast of this image (Fig. 2d) we find that the pure SBR shows a much stronger reflection of the light than the pure PB. The reasons for this enhanced intensity are a fine structure or concentration fluctuations caused by the styrene content of the SBR, which can be proven by using fluorescence LSCM [24].

The incident beam was sent in direction parallel to the interface. In this direction, however, the reflection of the light in the direction of the detector is very low [25]. The observed contrast of the interface can be enhanced by tilting the interface about the x-axis, in the set-up shown in Fig. 2a, such that the interface normal $\underset{\sim}{n}$ is tilted with respect to the x,y-plane – the scanning plane – as shown in Fig. 3a. In this case a certain fraction of the scattered beam and/or beam reflected at the interface with a sufficiently small angle $\alpha$ with respect to the $O_z$-axis can pass the pinhole. $\Delta F$ in Fig. 3a is the focal depth of the respective slices. To adjust the distance of the slices to the focal depth, so that every slice is mounted exactly on the other one, is quite difficult. In order to lose no information by having a gap between the successive slices, it is better to have an overlap region, $\Delta O$, of the focal depth $\Delta F$ between two subsequent slices, as shown in Fig. 3a. The two images (Fig. 3b) obtained from these two slices (Fig. 3a) will both show, besides the respective contrast of slice 1 and slice 2, the contrast generated in the overlap region. This overlap region (the green part of the image in panel Fig. 3b will become important for the discussion of the more complex morphologies discussed later.

Since the welded interface is not perfectly flat, as can be seen on the TEM micrograph (Fig. 2b), a certain fraction of this interface will have its normal vector $\underset{\sim}{n}$ oriented closer to the incident beam axis and will, therefore, show an increase in the amount of back scattered light at an angle smaller than $\alpha$, as illustrated in Fig. 3c.

### 3.2. Droplet morphology

Fig. 4a and b shown the transmission electron micrographs of the as cast samples with the compositions SBR/PB 70/30 (wt %/wt %) and 40/60 (wt %/wt %), respectively. The PB phase is more strongly stained by $OsO_4$ than the SBR. According to the composition the major component forms the matrix and the minor component forms droplets with an average diameter of about 700 nm for both mixtures. The LSCM images shown in Figs 5 and 6 of the two different samples 70/30 and 40/60 respectively, show the same features. Parts a show one slice in the x,y-plane along

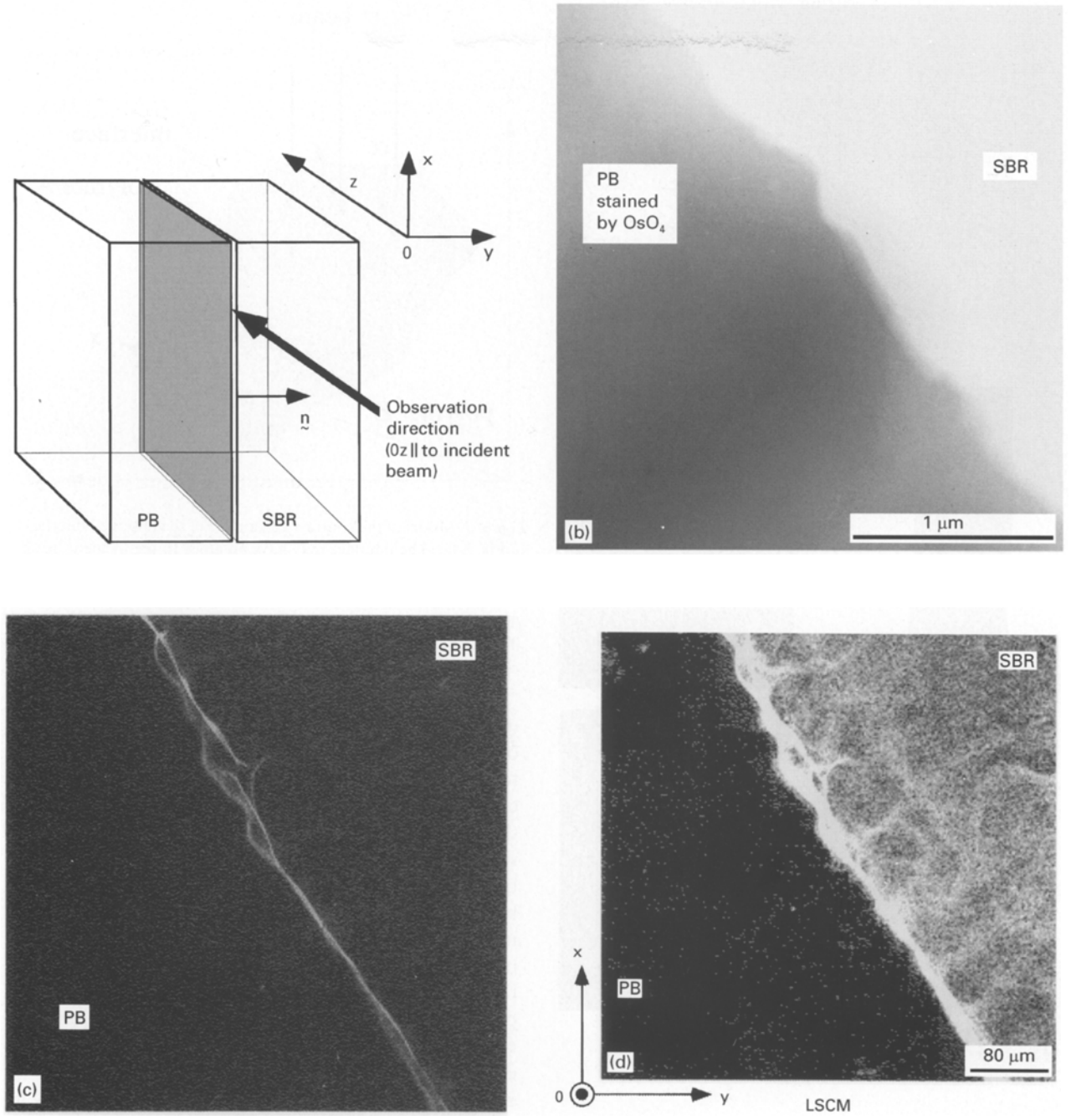


*Figure 2* Schematic representation (a), TEM (b) image and LSCM (c, d) image of the interface of a sandwich of pure SBR and PB. The x,y,z,-directions correspond to those of Fig. 1.

the long white lines in parts b and c, which are cuts in the y,z-plane and x,z-plane, respectively (compare Fig. 1). As it is mainly the interface which causes the contrast for both samples, the same contrast in the LSCM can be expected. In order to better understand the image generation, a more detailed geometric analysis shall be done later in the text.

The droplets found in the two samples have a size distribution with an average diameter close to the focal depth of the optical setup of about 700 nm (see appendix). Spheres with dimensions below the lateral resolution limit ($\approx$250 nm) of the microscope will not be seen or will contribute to the noise of the pictures. Spheres larger than the resolution limit can have a wide range of positions relative to the single slices and their overlap regions (see Fig. 3). Some representative orientation of droplets with different size shall be discussed.

Droplets with a diameter smaller than the scanning depth of a single slice, which do not share a surface with a neighbouring slice, are only visible in this slice; see the existence of such a particle in the series of white circles marked by arrow d in parts d to f in Fig. 7, where the droplet is only visible in part e (not depicted in Fig. 8 later). For a droplet with a diameter comparable to the focal depth, the two outermost positions relative to the focal limits of the single slices are depicted in Fig. 8a and b.

The droplet in Fig. 8a shares only an upper half with slice 2 while its lower half is located in slice 3 of Fig. 8. In the depicted slice series (Fig. 7a–h; notice that the steps between the single slices are 600 nm while they are 200 nm for Figs 5 and 6) such droplets are visible on two subsequent slices. From the top view (the image in x,y-plane) these spheres appear as small round discs with a diameter of about 300 to 400 nm as

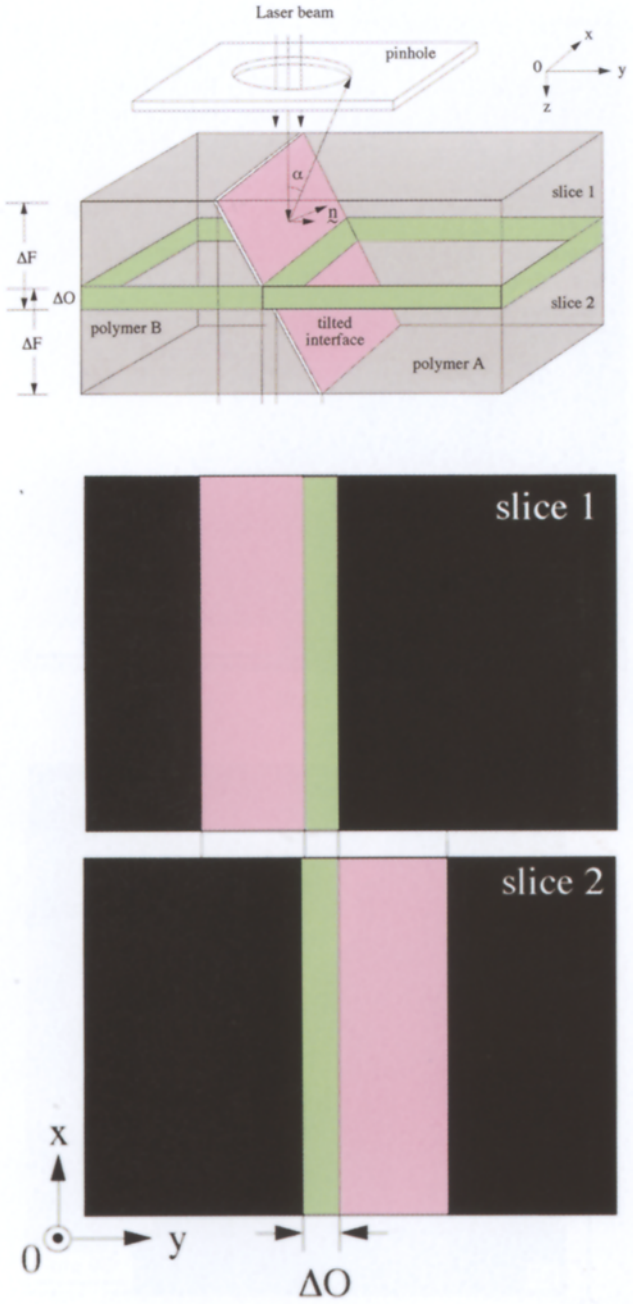


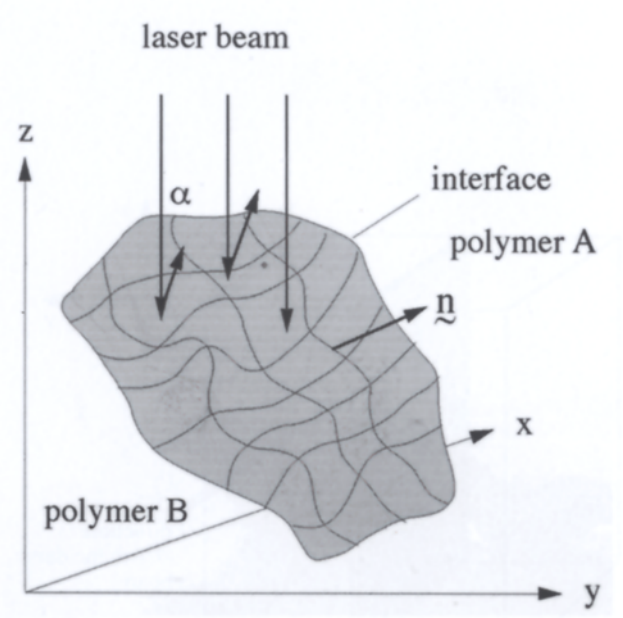


*Figure 3* Model of the contrast generation of the observed interface of Fig. 2. (a) The interface may have an angle to the incident beam which is sufficient to cause contrast on the detector. For simplification the objective lens between pinhole and sample is not depicted. (b) The interface images in slice 1 and 2. (c) Scheme of a wavy interface.

marked by an arrow b in Fig. 7f, g; although their original diameter should be around 700 nm according to our model. The contrast on slice 2 of Fig. 8a is caused only by the top surface A of the droplet while the bottom surface A′ is only visible in slice 3. When we follow the surface of the droplet from its top to bottom, we will reach a region where the angle between the normal vector of the interface and the incident beam becomes so large, that the scattering (reflection) angle $\gamma$ will become very large compared to the opening angle $\alpha$ of the aperture at the confocal point and no light will pass through the pinhole (see also Fig. 3) [25]. Therefore the middle part of the droplet is not visible (area C in Fig. 8a) and the diameter of the droplets observed in the LSCM image is smaller than the 700 nm $\cong \Delta F$, which can be expected from this model. As shown in Fig. 8a the area C is partially located in the overlap region of the two slices.

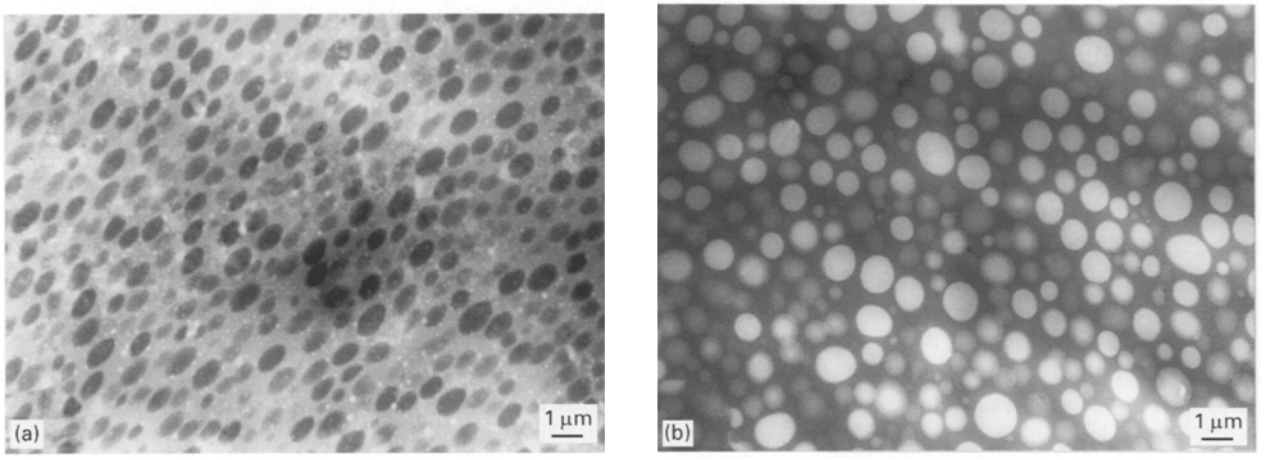


*Figure 4* TEM micrographs of the as cast samples of SBR/PB (a) 70/30 and (b) 40/60. The PB phase is selectively stained by $OsO_4$.

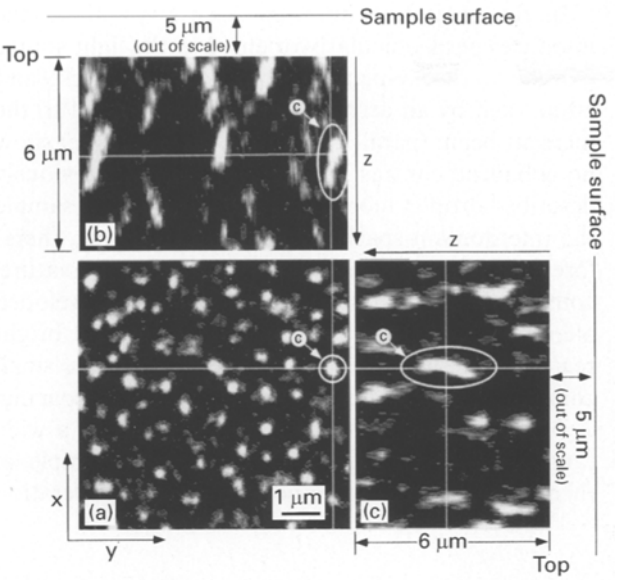


*Figure 5* LSCM image of SBR/PB 70/30 reconstructed from 30 slices with 200 nm distance (Magn. 100×, NA 1.4, effective pinhole size 43 µm, focal depth $\Delta F = 700$ nm). The white lines correspond to the lines where the three projections cut each other as can be seen from Fig. 1. The marked area with symbol c corresponds to a droplet which is artificially elongated by the scanning procedure as described in the text.

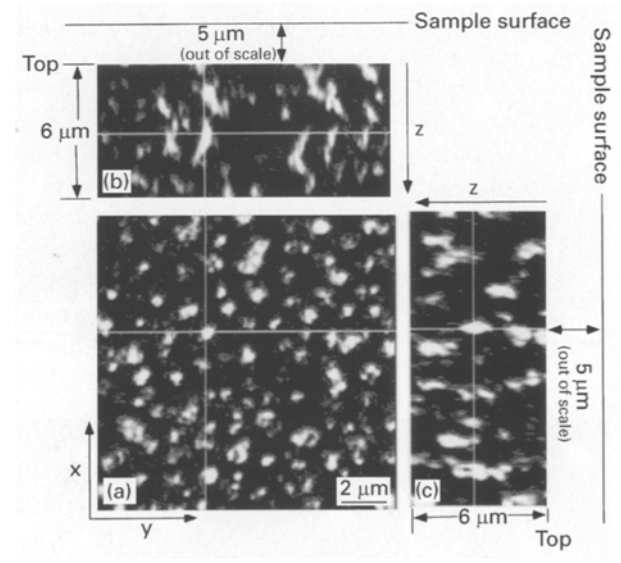


*Figure 6* LSCM image of SBR/PB 40/60 in Oxy-plane (a) and those in the z,y- (b) and z,x- (c) plane reconstructed from 30 slices with 200 nm distance (Magn. 63×, NA 1.4, effective pinhole size 26 µm, focal depth $\Delta F = 700$ nm). The white lines show the area where the images are cut as illustrated in Fig. 1.

As no light is back scattered from this area, the overlap region has no further influence on the image generation in this case.

When doing the reconstruction of the morphology in the direction of the x,z- or y,z-plane the subsequent slices are mounted one upon the other. One slice represents the whole focal depth and we cannot locate the position, i.e. height, of a reflection in this respective slice. This means that a droplet, although it occupies only a small fraction of the depth of the slice (compare red regions A in Fig. 8a and green areas A and B of the droplets in parts b and c respectively), will be given the same intensity throughout the whole slice, i.e. the thickness of one slice corresponds to 700 nm, but the visible height of the upper or lower part of the droplet is only half or less. Owing to the applied image processing, however, we get the impression that the reflection appears throughout the whole slice. The projection onto the x,z- or y,z-plane (Figs 5 and 6) gives therefore, not the impression of a sphere, but shows a kind of rod-like structure (see Fig. 5, the circle marked by an arrow c in x,z- or y,z projection).

In the case of the droplet shown in part b of Fig. 8, having the same diameter as sphere a, 700 nm $\cong \Delta F$, the top part of the droplet just touches the top surface of slice 2 at one point and the bottom part the bottom surface; the upper and the lower parts locate in the overlapping regions $\Delta O$ of the slices 1,2 and 2,3, respectively. The main back scattering occurs therefore in the overlapping regions. These overlap regions are due to the fact that the 600 nm scanning steps are, in this case, about 100 nm smaller than the focal depth $\Delta F$ of 700 nm. Therefore, slice 1 shows contrast caused by area A, slice 2 shows contrast caused by area A and A′ and slice 3 contrast caused by area A′. In the x,z or y,z projection such droplets appear even more elongated than in the previously discussed case of Fig. 8a, as the droplet is visible on three successive slices. The area C in the non-overlapping portion of slice 2 is not visible for the same reason as discussed for part b. If there is any other position of droplets of this size possible their appearance in the images will be in between these two extremes.

For larger spheres only one example position shall be discussed. When the diameter of the droplet is about two times larger than the focal depth, it is visible over three slices, as shown in Fig. 8c. Its location corresponds to that of droplet in Fig. 8b, but as its diameter is larger the top and bottom part occupy also space in the non-overlapping regions of slice 1 and 3. As the radius of the droplet becomes larger the curvature of the top and bottom part is smaller compared to the smaller droplet in Fig. 8b and the fraction of mainly reflecting area is increasing. A part of the upper or lower core (A and A′), the surface of which has an angle to the light source, which is still big enough to cause sufficient back scattering, is visible on slices 1 and 3 as a bright spot. In slice 1 the additional upper part B and in slice 3 the lower part B′ of the droplet are also visible. In slice 2 the centre C of the droplet will appear dark as it contains no reflecting interface and only the areas B and B′ cause the observed contrast. Such a case can be seen and marked by an arrow a in the original LSCM image (Fig. 7b, c, d or e, f, g). The droplet does not appear as a perfect circle on the centre slice, which may be due to local deformation or an ellipsoidal shape. The side of the droplet is not visible as described above and therefore the observed diameter is smaller than the actual size of the droplet.

### 3.3. Bicontinous morphology

The as cast sample of the 50/50 mixture has a bicontinous morphology with an average domain spacing of about 5 µm evaluated from its light scattering pattern.

This sample shows the phase-separated structure formed by spinodal decomposition, leading to continuously growing domain spacing with time. A detailed discussion of this process will be given elsewhere [21]. The structures developed are those in the late stage SD process.

The sample was kept for over 11 months at room temperature, which led to an increase of the domain spacing to about 25 μm, as visible in the LSCM image. The contrast generation of a bicontinous structure in the LSCM is complex. Figs 9 and 10 show the LSCM images of the as cast sample and the sample allowed to phase separate for 11 months, respectively. In both cases an interconnected structure is visible. Parts of a show, as in Figs 5 and 6, one slice in the x,y-plane along the long white lines in parts b and c, which are cuts in the x,z and y,z-plane, respectively (compare Fig. 1).

In the projection onto the x,z- or y,z-plane, the interfaces perpendicularly oriented to the light source (parallel to the x,y-plane) are clearly visible (Figs 9 and 10 marked by an arrow (i)). Interfaces parallel to the incident beam (parallel to the z,x- or z,y-plane) show no enhanced contrast, as observed for the previously described droplet morphology. For the as cast sample the interdomain spacing is much smaller and, therefore, the structures show a much stronger curvature, compared to the phase separated structure developed after 11 months. Therefore, the extension of a bright region of the interface in one direction is quite small compared to the sample with larger domain spacing.

The interconnection of each phase leads to a wide range of different local structures. One example of them is a tetrapod unit and the contrast generation

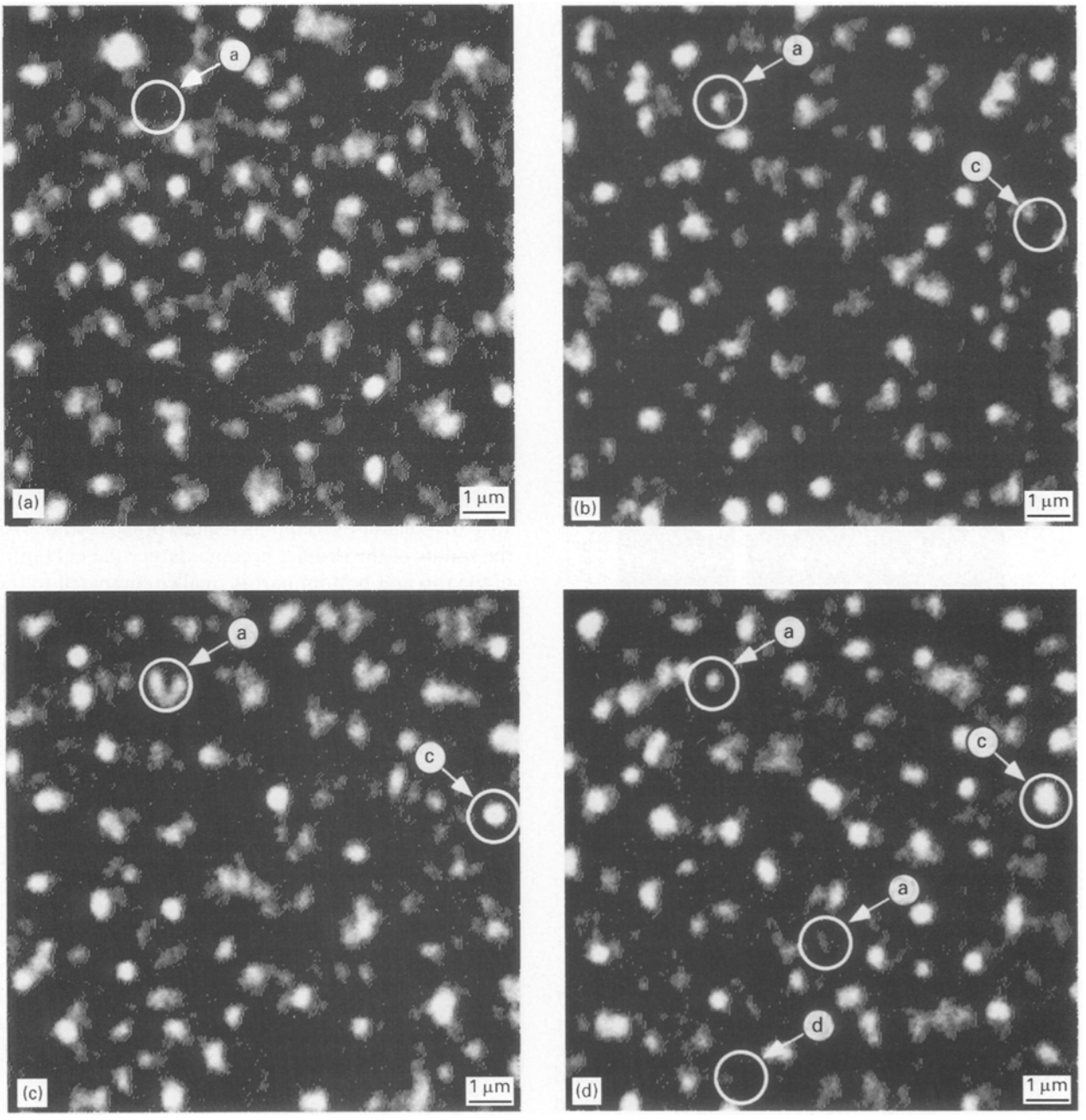


*Figure 7* A LSCM image series of about 700 nm (≡ ΔF) thick slices with a distance between two successive slices of 600 nm of SBR/PB 70/30 corresponding to Fig. 5a. The encircled areas a,b,c and d correspond to droplets causing a different kind of contrast generation, as schematically illustrated in Fig. 8. (a) 10 μm from top surface; (b) 10.6 μm; (c) 11.2 μm; (d) 11.8 μm; (e) 12.4 μm; (f) 13.0 μm; (g) 13.6 μm; (h) 14.2 μm.

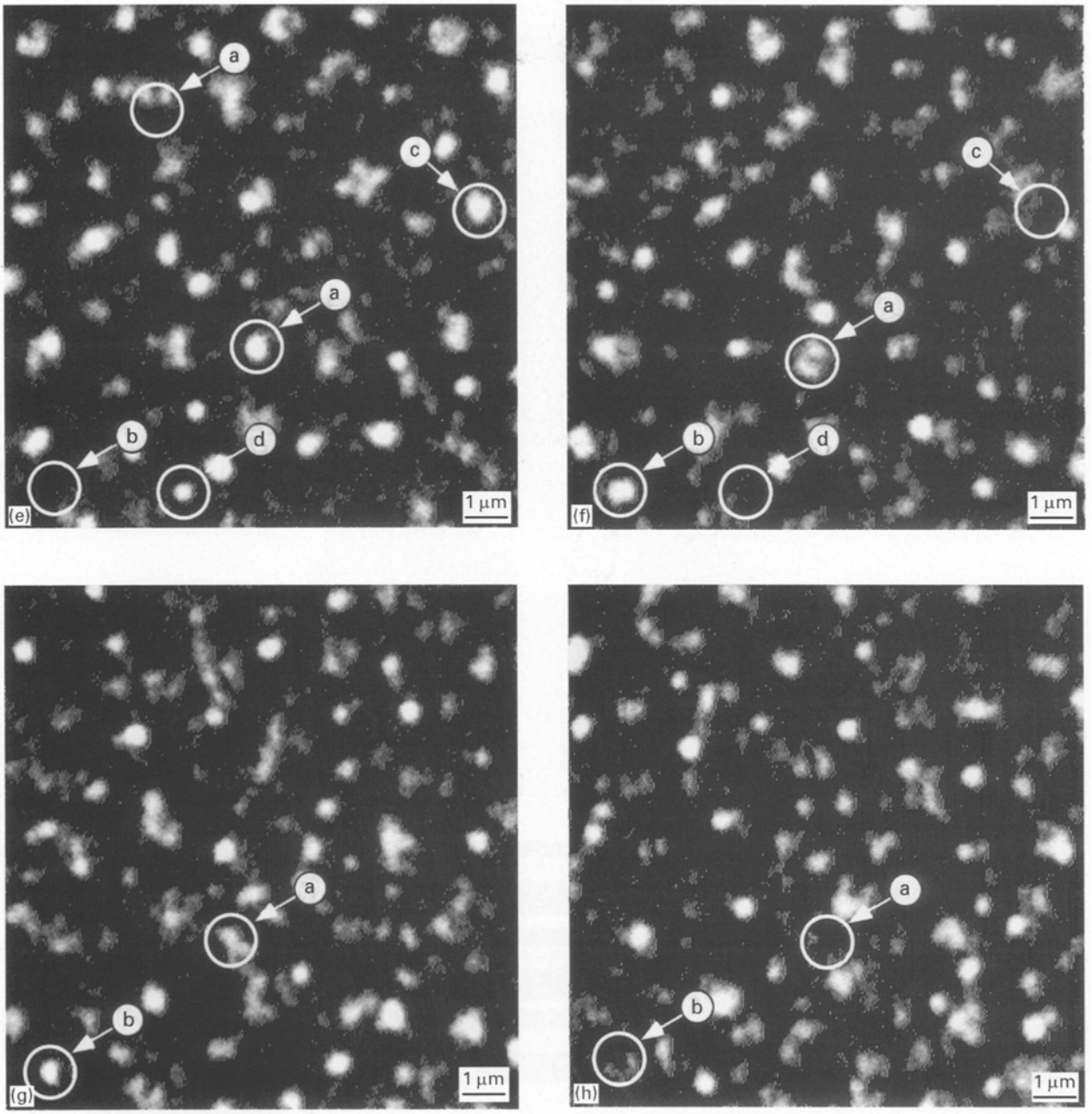


*Figure 7* (Continued)

will be discussed using this morphological unit. The interface of the tetrapod unit can have any orientation relative to the incident beam. One possible alignment relative to the laser axis is given in Fig. 11a. A certain area A of the interface on the upper side of the tetrapod is mainly perpendicular to the incident beam. This area will therefore cause strong back scattering and result in a strong contrast on the LSCM image [25]. Such areas are clearly visible in the region marked by an arrow t in Fig. 9. By changing the scanning depth, these areas rapidly become out of focus and are not visible on the slice above or below, except when this interface is located in the overlap region of two successive slices. In this case it will be seen on both slices. It should be mentioned that it makes no difference in the LSCM image if the tetrapod is oriented, as drawn in Fig. 11a, or stands upside down. In both cases the interface will have the same angle relative to the incident beam.

The parts (b) and (c) in Fig. 11 shows a cut-out of a single tetrapod unit directly observed by LSCM. The original observed contrast and the images obtained after noise filtering are given in parts b and c, respectively. The upper images corresponding to slice 1 clearly show the highest intensity in area A of the tetrapod unit, which is oriented perpendicular to the incident beam. When we follow this unit in z-direction we reach an area (slice 2), where the local structure becomes tubular. In the LSCM we observe a circular shaped area with a noisy contrast (Fig. 11b lower image). This area corresponds to the SBR as can be concluded from the experiment in Section 3.2 and investigations on this system by fluorescent LSCM [24]. Accordingly the grainy structure visible in the SBR might be caused by a fine structure or

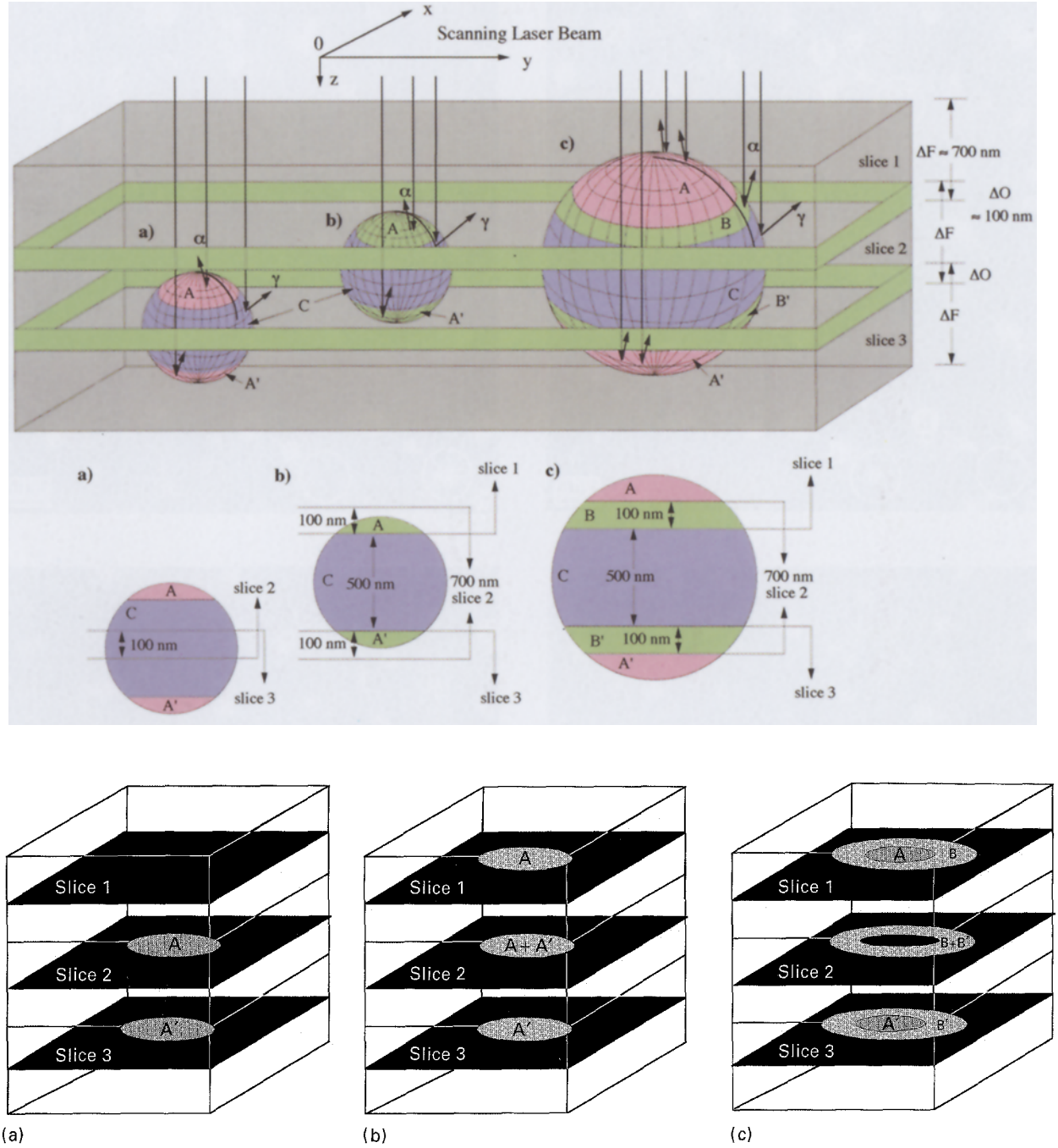





*Figure 8* Model with three examples of the position of droplets relative to the positions of the single slices obtained by LSCM, which explains the contrast generation on the LSCM images of Figs 5, 6 and 7 a–h. ΔF is the focal depth and ΔO is the overlap region of the subsequent slices. The angle α corresponds to the opening angle of the pinhole aperture and γ indicates any angle of the back-scattered light which will not pass through the pinhole at the confocal plane and not reach the detector. The sketches in the middle show a two-dimensional view of the y,z-plane and the sketches below, the expected contrast of the LSCM images for the three different cases.

concentration fluctuations caused by the styrene content of the SBR. The contrast generation of the SBR region is expected to be due to back scattering rather than reflection at the interface.

This enhanced contrast of the SBR allows us to obtain a perfect three-dimensional reconstruction of the bicontinous structure after noise reduction of the original LSCM image. An example is depicted in Fig. 11b, c. A sample with 50/50 composition, which was first homogenized and then annealed for 2 days at 100 °C, shows a very regular bicontinous morphology with a domain spacing of about 10 μm measured by light scattering. From 30 single slices with a step size of 500 nm, a three-dimensional model, as seen in Fig. 12a, was reconstructed. The depicted area in part a has a depth of 15 μm and therefore the dimension of 1.5 repeat units. The parts b and c are two-dimensional cuts along the white (inner pictures in parts b and c) or blue lines (outer pictures in parts b and c) in direction of the z,y- and z,x-plane respectively. The green and red arrows mark points with the same location on the three different views. As clearly visible from Fig. 12, both phases are perfectly interconnected. The coloured phase (white-to-purple colours) represents the SBR, while the PB phase is shown in black. To obtain the three-dimensional impression for the eye in

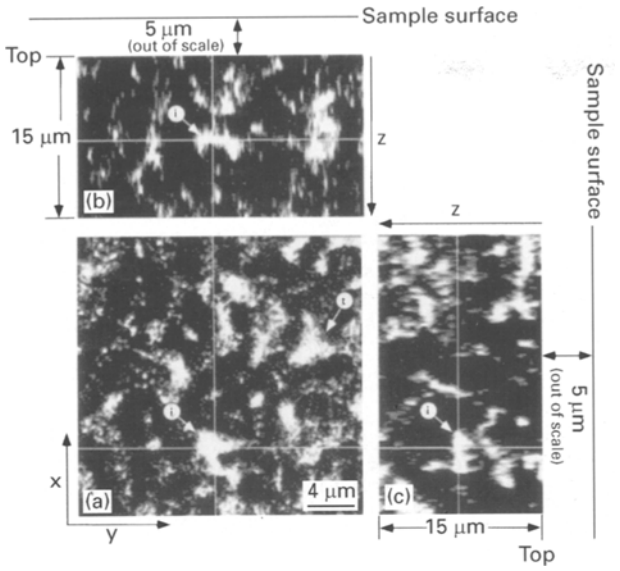


*Figure 9* LSCM image of SBR/PB 50/50 as cast from solution with bicontinous morphology in the Oxy-plane (a) and those in the z,y- (b) and z,x- (c) plane reconstructed from 30 slices with 500 nm distance (Magn. 63 ×, NA 1.4, effective pinhole size 35 µm, focal depth $\Delta F = 800$ nm). The area marked with i corresponds to an interface which is oriented perpendicular to the incident beam.

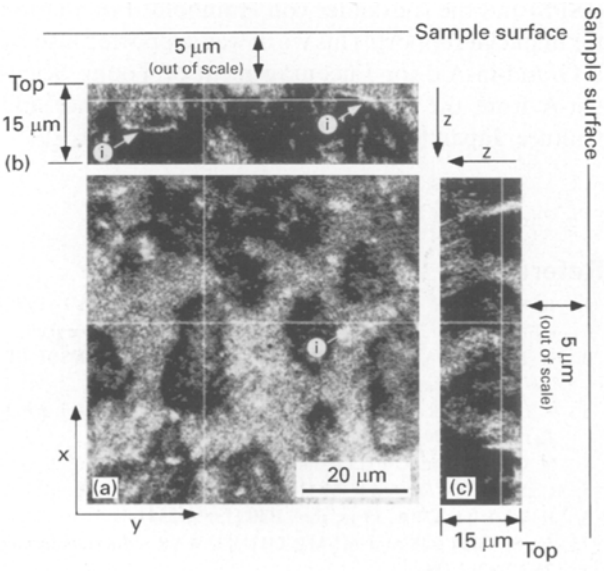


*Figure 10* LSCM image of SBR/PB 50/50 left for 11 months at room temperature showing bicontinous morphology in Oxy-plane (a) and those in the z,y- (b) and z,x- (c) plane reconstructed from 30 slices with 500 nm distance (Magn. 63 ×, NA 1.4, effective pinhole size 52 µm, focal depth $\Delta F = 1100$ nm). The area marked with i corresponds to an interface which is oriented perpendicular to the incident beam and shows strong reflection.

part a, the intensities of the single slices were not normalized during the scanning process: the reflection of the top slice is much stronger than the reflection of the slices further away from the light source (the laser has to pass more solid material and therefore loses more intensity when going in direction to a slice which is further away as well as on its way back to the detector (see also Fig. 1). The change of the colour from white to purple corresponds therefore mainly to a loss of intensity in direction of the z-axis into the

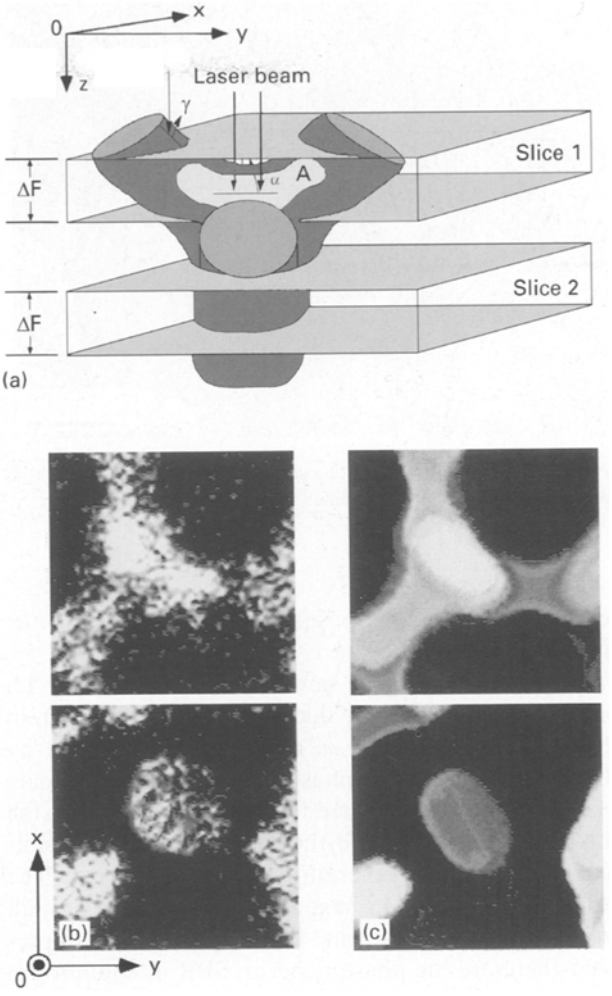


*Figure 11* Model for the orientation of a tetrapod structure unit (a) contained in a bicontinous structure with no long range order and cut-outs of the LSCM slices original image contrast enhanced (b) and noise reduced (c) representing slices 1 and 2. The upper bright area A shows strong reflection in direction to the detector and appears therefore bright on the LSCM image.

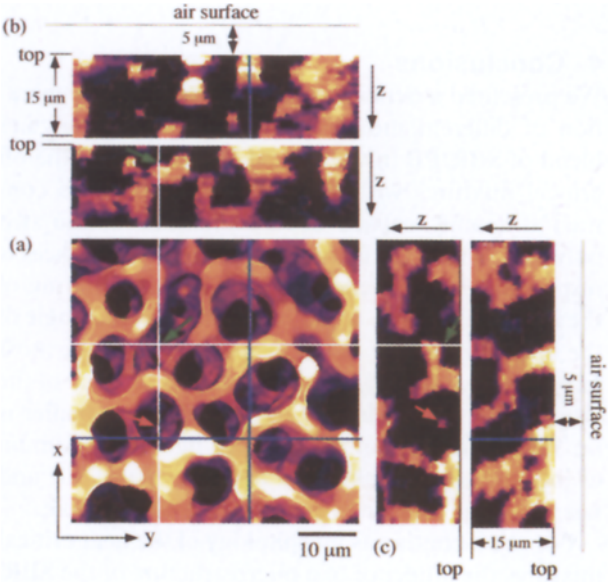


*Figure 12* (a) 3D-reconstruction from 30 LSCM slices with a distance of 500 nm (Magn. 63 ×, NA 1.4, effective pinhole size 35 µm, focal depth $\Delta F = 800$ nm); the white or blue lines show the cutting direction where the images (b) and (c) were obtained (see sketch in Fig. 1).

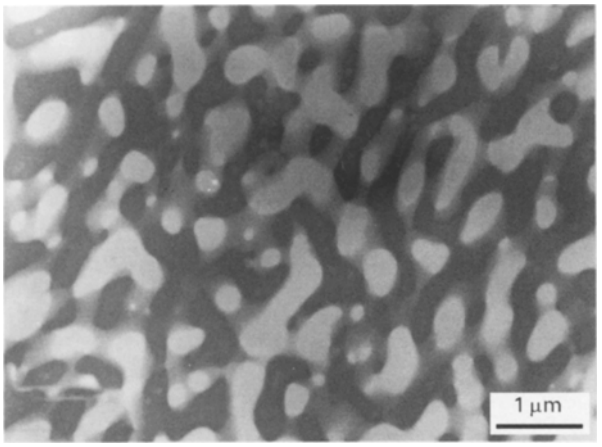


*Figure 13* TEM micrograph of a sample annealed for 1 h at 100 °C after homogenization and stained by $OsO_4$.

depth, which is superposed by the reflection of the interfaces parallel to the x,y-plane.

A TEM image of the same sample annealed for 1 h at 100 °C with a sample thickness of 50 nm is given in Fig. 13. The PB phase is more strongly stained by $OsO_4$ than the SBR phase and, therefore, appears dark, as can be concluded from Fig. 2b. Although the LSCM sliced image and the TEM pictures look similar, the contrast generation is quite different. The contrast in the TEM image is caused by a low or high content of staining agent. The brightest areas represent therefore the phase richer in SBR in equilibrium composition throughout the whole depth of the sample. In the LSCM image, however, an area with maximum intensity represents only an interfacial area which is perpendicular oriented to the incident beam. As is clearly visible from the TEM image (Fig. 13) the brightest SBR-rich areas are connected by tubular structures with lower brightness (grey contrast) proving the bicontinuity of the structure.

## 4. Conclusions

We presented a detailed analysis of the image generation of different morphologies of a binary polymer blend of SBR/PB in the LSCM. In the case of the off critical mixtures with droplet morphology the contrast is mainly caused by the interface of the two polymers, where the change of the refractive indices is responsible for the reflection and/or the scattering of the incident beam. It could be shown that the angle of the interface relative to the incident beam is the most important parameter. The larger the local angle of the interface to the incident beam becomes the smaller is the reflection angle of the reflected light. A maximum of intensity can be observed for an angle of 90° and nearly all the reflected light can pass the pinhole.

For the bicontinous morphology of the near critical mixtures the influence of a microstructure of the SBR, which is described in detail elsewhere [24], becomes important and causes additional contrast to the reflection of the interface of the two polymers. Finally the described phenomena are useful for the analysis and interpretation of the structures of this blend developed via spinodal decomposition, which will be described in a forthcoming work [21].

## Appendix

The focal depth $\Delta F \equiv$ HMW of the slices was determined by using the following equation, which is especially usable for this kind of microscope. More detailed information can be found elsewhere [11].

$$\text{HMW}\ [\mu\text{m}] = [2\,nph/1.75\ \text{Magn.}\,\text{NA} + n\lambda/\text{NA}^2 \times \exp(-2\,NA\,ph/1.75\,\lambda\ \text{Magn.})]$$

where HMW = half maximum width of the optical section; $n$ = refractive index of the immersion medium (1.52); $ph$ = effective pinhole size in µm; Magn. = magnification (here 63 × and 100 ×); $NA$ = numerical aperture (here 63 ×, NA = 1.4; 100 ×, NA = 1.4); $\lambda$ = wavelength of the used laser source (here 0.633 µm).

## Acknowledgements

The authors would like to thank Professor H. Hasegawa for helpful discussions. A.R. would like to thank the Japanese Society for Promotion of Science (JSPS) and the Alexander von Humboldt Foundation for financial support. This work was supported also by a Grand-in-Aid for Encouragement of Young Scientist-A from the Ministry of Education, Science and Culture, Japan (Grant Nr. 00093202).

## References

1. B. S. KIM, T. CHIBA and T. INOUE, *Polymer* **36/1** (1995) 43.
2. H. M. SHABANA, W. GEO, R. OLLY and D. C. BASSETT, *Polymer Commun.* **34/6** (1993) 1313.
3. J. LAEUGER, R. LAY and W. GRONSKI, *J. Chem. Phys. Lett.* **10/8** (1994) 7818.
4. Y. OONO and S. PURI, *Phys. Rev.* **A38** (1988) 434.
5. C. YEUNG, *Rev. Lett.* **61** (1988) 1135.
6. H. FURUKAWA, *Phys. Rev.* **B40** (1989) 2341.
7. M. A. KOTNIS and M. MUTHUKUMAR, *Macromolecules* **25** (1992) 1716.
8. T. KOGA and K. KAWASAKI, *Phys. Rev.* **A44** (1991) 817.
9. M. TAKENAKA and T. HASHIMOTO, *Phys. Rev. E, Rapid Commun.* **48** (1993) 647.
10. J. L. LICHTMANN, *Sci. Amer.* **8** (1994) 30.
11. T. WILSON, "Confocal microscopy" (Academic Press, London, 1990); Product specification ZEISS LSM 320.
12. H. VERHOOGT, J. VAN DAM, A. POSTKUMA DE BOE, A. DRAAIJER and P. M. HAUPT, *Polymer* **34** (1993) 1325.
13. L. LI, S. SOSNOWSKI, C. E. CHAFFEY, S. T. BALKE and M. A. WINNIK, *Langmuir* **10** (1994) 2495.
14 H. JINNAI, Y. NISHIKAWA, T. KOGA and T. HASHIMOTO, *Macromolecules* **28** (1995) 4782.
15 T. IZUMITANI and T. HASHIMOTO, *J. Chem. Phys.* **83(7)** (1985) 3694.
16. T. IZUMITANI, M. TAKENAKA and T. HASHIMOTO, *J. Chem. Phys.* **92(5)** (1990) 3213.
17. M. TAKENAKA, T. IZUMITANI and T. HASHIMOTO, *ibid.* **92(7)** (1989) 4566.
18. T. HASHIMOTO, T. IZUMITANI and M. TAKENAKA, *ibid.* **97(1)** (1992) 679.

19. M. TAKENAKA, T. IZUMITANI and T. HASHIMOTO, *ibid.* **98(4)** (1993) 3528.
20. J. W. CHAN, *ibid.* **42** (1965) 93.
21. A. RIBBE and T. HASHIMOTO, *Macromolecules* (to be submitted).
22. T. HASHIMOTO, T. IZUMITANI and M. TAKENAKA, *Macromolecules* **22** (1989) 2293.
23. A. RIBBE and T. HASHIMOTO, *Macromolecules* (to be submitted).
24. H. JINNAI, H. YOSHIDA, K. KIMISHIMA, Y. HIROKAWA, Y. FUNAKI, A. RIBBE and T. HASHIMOTO, *Macromolecules* (submitted).
25. P. C. CHENG and G. R. SUMMERS, in "Handbook of biological confocal microscopy", edited by J. D. Pawley (Plenum Press, New York, 1990) Chapter 17, p. 179.

*Received 20 November 1995*
*and accepted 13 June 1996*